Adaptive Power Control Based on Neural Network Design and Implementation for the Hybrid Shipboard Microgrids

Farooq Alam, Arsalan Rehmat, Syed Sajjad Zaidi, Bushra Raza, Maryam Arshad, Muhammad Abdullah
(farooq.phdee19pnec, arsalan.msee19pnec)@student.nust.edu.pk, sajjadzaidi@pnec.nust.edu.pk
Department of Electronics and Power Engineering,
National University of Sciences and Technology, Islamabad, Pakistan

***Abstract*—With the increase in carbon emissions, climate change, and reduction in fossil fuels, there is a need for energy storage systems and renewable energy sources for ships and ferries. Currently, seaports do not have shore-based cold ironing facilities in most ship ports. Therefore, electricity is provided by the main grid. Due to the lack of a cold ironing facility on the ship, expansive diesel generators must be equipped on the ship. Furthermore, the ship must be functional to provide supply to auxiliary loads on the ship. To provide a solution to these issues, we need to provide cold ironing facilities to every seaport. However, this solution will take time to implement, and it will be very costly. On the other hand, ship-based microgrid systems will enable clean and economical power generation facilities on the ship. The idea is to implement a low-cost hybrid microgrid system on the ship so that we receive alternate energy resources. We proposed a nonlinear droop control design for the improvement of voltage and frequency droops in the bidirectional power converter model. A comparison of conventional and proposed control designs has been presented in simulation results. Hardware implementation on the Jetson Nano system and practical results have been validated.**

***Index Terms*—Artificial Intelligence, Adaptive Control, AC and DC loads, Hierarchical Control Designs, Neural Networks, Shipboard Microgrids.**

I. Introduction

A hybrid Microgrid (MG) consists of alternating current (AC) and direct current (DC) systems connected by extensive multidirectional converters. With such a system, the conversion stages, that is DC-AC-DC and AC-DC-AC, in a separate DC or AC microgrid can be abridged. The AC sources and loads of such a microgrid are connected to the AC MG bus, and the DC loads and sources are coupled with the DC busbar, and any of the MGs can be connected to the interconnected load or equipment [1].

Figure 1 depicts the single-line diagram of a ship-based hybrid AC/DC microgrid. The architecture of the hybrid AC/DC microgrid consists of various AC and DC sources, which include renewable energy sources (RES), battery banks, and interconnected loads on the distribution side. Diesel generators, battery banks, solar panels, and wind turbines, linked with respective bus bars [2].

The MG supplies or utilizes the main grid to attain load demand in grid-connected operation and power generation MGs must be able to execute grid isolation when load variations or disturbances occur. However, the MG executes efficiently during operation mode to ensure that the critical load supply is not interrupted. The transients that occur during the switching phase must be well managed to avoid device obliteration [3].

It is possible to form a seaport microgrid by integrating numerous shipboard Microgrids (SMGs) with distributed control, along with an on-shore charging structure. It is called a ship-based seaport microgrid because it integrates numerous SMGs and charging stations with ports. Furthermore, data communication methods are employed to share power among different microgrids, which reduces the system's cost and complexity [4]. On the other hand, a decentralized droop-control technique, as well as power division among SMGs in both charging and discharging modes is anticipated using a multimode microgrid. Electricity is supplied or consumed depending on the State of Charge (SoC) of battery banks [5].

Using a decentralized droop-control technique, power division among SMGs in both charging and discharging means is anticipated using a multimode. Electricity is supplied or consumed depending on the SoC of battery banks [6]. For many years, ships have been powered by electric motors. There has been a shift at the beginning of the electric-based ship in which electric propulsion (electric equipment) is linked to the electrical grid for fuel efficiency improvement and lowered emissions [7]. Nevertheless, diesel generators remain the principal source of electricity onboard. To meet the load, additional generators are linked in parallel [8]. The generator loading is not effective during low load factor operation of the generator or a higher specific fuel consumption (SFC) curve, owing to the nonlinear nature of thermal units, such as diesel generators [9].

The shipboard microgrid consists of some types of power sources. The shipboard microgrid comprises wind turbines (WT), distribution generator (DG), photo-voltaic (PV), battery systems, and connected loads on both sides, as depicted in Figure 1. There are two kinds of power sources that are non-dispatchable sources (PV, WT) and dispatchable sources (DG, Battery Energy Storage Systems (BESS)) [10]. Shipboard microgrids are typically operated on an island model. An adaptive controller is employed in the research discussed in

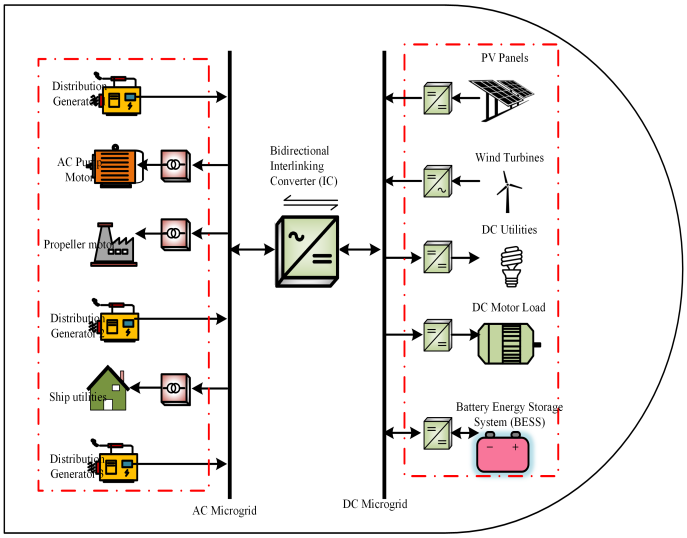

Fig. 1: Single Line Diagram of the shipboard-based hybrid AC/DC microgrid

[11] to determine the outputs at each hour of the day for controllable power sources. The energy management system (EMS) will forecast PV and WT output power as well as load requirements for the next day [12].

Second, dispatchable source outputs are determined based on the SoC and information on the battery scheme to calculate the microgrid's total losses. Moreover, the battery charging and discharging losses, as well as the fuel costs, ought to be considered [13]. It functions very rarely in grid-connected mode, which is dissimilar from terrestrial microgrids [14]. A smart microgrid architecture is made up of several smart microgrids that are connected by an effective controller and may either be incorporated into the grid or run separately.

A multi-microgrid connects residential, commercial, and industrial load centers to a wide range of renewable and non-renewable energy sources. The statistical analysis of the collected data on consumer energy usage and weather forecasts for different RESs is essential for real-time electric power system management and requires data analytics and artificial intelligence (AI) approaches [17]. However, several modules, including tariff [18] control and power flow management, work together to assess data collected from power consumers by the AI-based controller [19].

The creation of a smart microgrid system with several RESs interconnected with the electrical power grid is the main novelty of this study. The shipboard Interlinking Converter (IC) serves as the foundation for the adaptive control mechanism proposed here. Using a fuzzy logic controller (FLC), this algorithm was improved and made more intelligent by taking into consideration many characteristics [20] relating to the main power grid, microgrid, source current, and load demand. This idea may be used for as many microgrids as needed to regulate power flow and improve power quality. An in-depth analysis of the suggested adaptive-based intelligent controller for active energy-sharing and reducing power quality concerns under unbalanced nonlinear load is detailed in this research work.

This paper introduces an innovative adaptive neural network (NN)-based control scheme for hybrid AC/DC microgrid systems, marking a significant advancement in the integration of AI with power system management. The novelty of this work lies in its unique approach to combining AC and DC elements within a microgrid, enhancing system flexibility and efficiency shown in Figure 2. The adaptive NN based control scheme leverages advanced functionalities such as decision-making, machine learning, and inference to address the complex control problems inherent in hybrid microgrids. This research distinguishes itself by presenting a comprehensive comparative study that demonstrates how AI integration improves the stability and performance of hybrid microgrids. The practical validation through simulations further underscores the effectiveness of the proposed intelligent control scheme, highlighting its potential to revolutionize the operation and management of modern power systems.

The study of this research is divided into the following sections. The components and procedures of the microgrid system with several microgrids connected to RES are explained in Section 2. The performance of the suggested microgrid system with the IC and its significance in the developing research area are briefly discussed in Section 3. A thorough discussion of the smart microgrid model's economic viability is also included. Results are presented in Section 4, along with design verification and testing of the suggested smart microgrid system employing adaptive control that is intelligently incorporated into hardware platforms and simulations. Hardware results are elaborated in section 5, followed by section 6, which concludes with observations and provides future recommendations.

II. The Shipboard Microgrid Modeling

Research [20] examines a small ferry whose architecture is based on a multiple hybrid circuit with AC/DC systems distribution. Therefore, there is no direct mechanical link between the engines and the propulsion system. This ship is 22.5 meters in length, carrying payload from one station to another, and is situated 650 meters away [21].

Step-down transformer 440/230V connects this AC bus to the propulsion load or ship service loads. On the DC bus, battery, WT, PV, and connected load. Pumps, emergency switchboards, control units, safety systems, and lighting panels are linked to a bidirectional DC/DC converter and DC bus, respectively [22].

A. AC Microgrid Modeling

MG is classified as AC, DC, or hybrid AC/DC systems. In Figure 1, AC sources have been connected with the AC busbar network in the AC Microgrid. Usually, microturbines, diesel engines, and WT generators can be directly joined to the AC busbar in the absence of converters [23]. In contrast, DC power supplies such as batteries, energy storage system (ESS), and solar panels require an AC/DC inverter. In this way, all loads are linked to the AC busbar in a straight line. AC MG

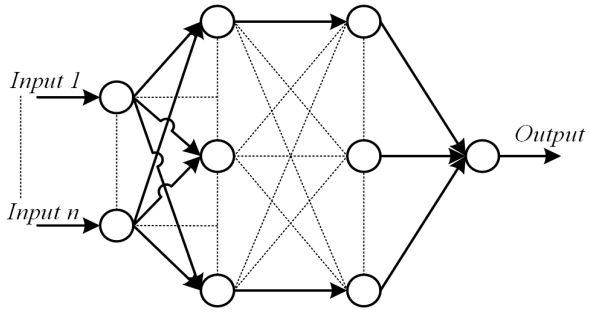

Fig. 2: Structure of neural networks

has numerous disadvantages, and such a system is difficult to control and synchronize [24].

The point of common coupling (PCC) is in charge of managing power between the main AC source and the main grid. Usually, three-phase AC buses assist as PCCs, and between the main power grid and the MG, a fast switch is employed as a cutoff point [25]. The DG will yield enough power to power the load and then send the surplus power to the grid under standard conditions [27]. The chief grid will control and transmit the power essential to the AC MG once the output power production by the DGs is less than that of the load demand [27].

B. Electrical Load

Table I shows that the rating of maximum propulsion loads, ship service loads, pumps, emergency switch boards, control units, safety systems, lighting panels. In cruise ships that run at fractions of their rated load mostly, electric propulsion can be superior to mechanical alternatives because of potential fuel savings and high maneuverability [28]. Highly precise torque response and higher over-torque capacity were understood to be necessary for ice-breaking applications and dynamic positioning in drilling boats. Figure 3 shows the flow diagram of the Adaptive control scheme for the hybrid shipboard microgrid [29].

Consider a static R_{load} and L_{load} are linked to the AC microgrid. The DGs kind of AC power source powers the load. We may use Kirchhoff's Voltage Law (KVL) on the AC source side to get the dynamic equations for the AC microgrid. In literature [30], the research will offer a hierarchical control system for DG units that consists of two levels. The first level includes primary controls that are based on droop, and the second level includes secondary controls that restore voltage and frequency parameters [31]. The voltage across the transmission line impedance and the associated AC load voltage. The source side equation may be expressed as

$$V_{i,ac} = \{i_{i,ac}R_{i,ac} + V_{i,ac}\} + V_{i,ac,load} \tag{1}$$

where voltage across line impedance is the rate of change of line inductance.

$$V_{i,ac} = L_{i,ac}\frac{\mathrm{d}}{\mathrm{d}t}i_{i,ac} \tag{2}$$

so, (1) can be written as

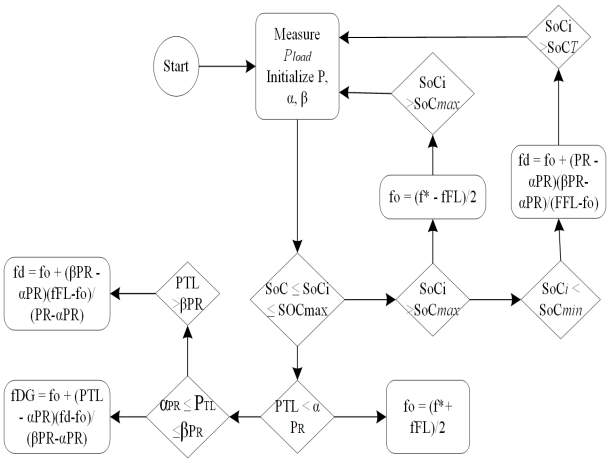

Fig. 3: Flow diagram of Adaptive control scheme

$$V_{i,ac} = \{i_{i,ac}R_{i,ac} + L_{i,ac}\frac{\mathrm{d}}{\mathrm{d}t}i_{i,ac}\} + V_{i,ac,load} \tag{3}$$

By rearranging (3), we get

$$\frac{\mathrm{d}}{\mathrm{d}t}i_{ac,line} = \frac{1}{L_{ac,line}}(V_{ac,s} - V_{ac,line}) - \frac{R_{ac,line}}{L_{ac,line}}i_{ac,line} \tag{4}$$

Now, AC load side equation is the summation of voltages across load impedance.

$$V_{i,ac} = i_{i,ac,load}\ R_{i,load} + V_{i,L_{load}} \tag{5}$$

where

$$V_{i,L_{load}} = L_{load}\ \frac{\mathrm{d}}{\mathrm{d}t}i_{i,ac,load} \tag{6}$$

so, (13) can be written as

$$V_{ac,load} = i_{ac,load}\ R_{load} + L_{load}\ \frac{\mathrm{d}}{\mathrm{d}t}i_{ac,load} \tag{7}$$

By rearranging (7), we get

$$\frac{\mathrm{d}}{\mathrm{d}t}i_{ac,load} = \frac{V_{ac,load}}{L_{load}} - \frac{R_{load}}{L_{load}}i_{ac,load} \tag{8}$$

The $d-q$ state space model for (4) and (8) of AC network can be given as

$$\frac{\mathrm{d}}{\mathrm{d}t}i^d_{ac,line} = \frac{1}{L_{ac,line}}\left(V^d_{ac,s} - V^d_{ac,load}\right) + \omega i^q_{ac,line} - \frac{R_{ac,line}}{L_{ac,line}}i^d_{ac,line} \tag{9}$$

$$\frac{\mathrm{d}}{\mathrm{d}t}i^q_{ac,line} = \frac{1}{L_{ac,line}}\left(V^q_{ac,s} - V^q_{ac,load}\right) - \omega i^d_{ac,line} - \frac{R_{ac,line}}{L_{ac,line}}i^q_{ac,line} \tag{10}$$

$$\frac{\mathrm{d}}{\mathrm{d}t}i^d_{ac,load} = \frac{V^d_{ac,load}}{L_{load}} + \omega i^q_{ac,load} - \frac{R_{load}}{L_{load}}i^d_{ac,load} \tag{11}$$

$$\frac{\mathrm{d}t^q}{i}_{ac,load} = \frac{V^q_{ac,load}}{L_{load}} - \omega i^d_{ac,load} - \frac{R_{load}}{L_{load}}i^q_{ac,load} \tag{12}$$

$$\dot{x}_i = A_i x_i + B_i u_i + D_i \tag{13}$$

where $A\ B\ C\ D$ can be found by

$$A = \begin{bmatrix} -\frac{R_{i,ac}}{L_{i,ac}} & \omega & 0 & 0 \\ -\omega & -\frac{R_{i,ac}}{L_{i,ac}} & 0 & 0 \\ 0 & 0 & -\frac{R_{i,ac}}{L_{i,ac}} & \omega \\ 0 & 0 & -\omega & -\frac{R_{i,ac}}{L_{i,ac}} \end{bmatrix} \tag{14}$$

$$B = \begin{bmatrix} \frac{1}{L_{i,ac}} & 0 \\ 0 & \frac{1}{L_{i,ac}} \\ 0 & 0 \\ 0 & 0 \end{bmatrix} \tag{15}$$

$$C = \begin{bmatrix} 1 & 0 & 0 & 0 \\ 0 & 1 & 0 & 0 \end{bmatrix} \tag{16}$$

$$D = \begin{bmatrix} -\frac{1}{L_{i,ac}} & 0 \\ 0 & -\frac{1}{L_{i,ac}} \\ \frac{1}{L_{i,ac}} & 0 \\ 0 & \frac{1}{L_{i,ac}} \end{bmatrix} \tag{17}$$

C. DC Microgrid Modeling

Most MG generators yield DC power, which ought to be transformed to AC for use with current AC lines. The DC to AC alteration is needed at the system's end since a few pieces of equipment need AC power to run. In AC MG, the DC-AC-DC energy conversion decreases efficacy and leads to substantial power losses [32]. DC MG offers considerable energy savings over AC MG by requiring fewer converters in one MG system. In addition to eliminating some control problems in the MG, DC MG ensures that DC bus voltage is largely responsible for the controls so that DG synchronization is no longer required. Additionally, as there is no need to manage reactive power flow, the primary control of the system is simpler. Modern devices use direct current instead of power electronics that can produce harmonics and create low levels of conversion because they skip the AC step in the intermediate process. A DC MG operates more smoothly than that of an AC MG because phase monitoring and frequency are not considered.

Research [33] demonstrates the model of a Low Voltage DC ship electrical scheme with variable speed generators and batteries and its application on the Opal-RT simulator. To understand the proper system's behaviour, it is increasingly vital to signify the whole component dynamics and relative control. It is becoming increasingly significant to employ digital twins to observe the behaviour of systems under all circumstances and inclusively.

The combination of a variable speed generator with a BESS is an effectual resolution for maximizing ship-based energy efficiency in a marine vessel. The study conducted in [34] aims to discover how DC-based shipboard power circulation compares to conventionally used AC solutions. Present concepts, emerging initiatives, and design challenges are observed

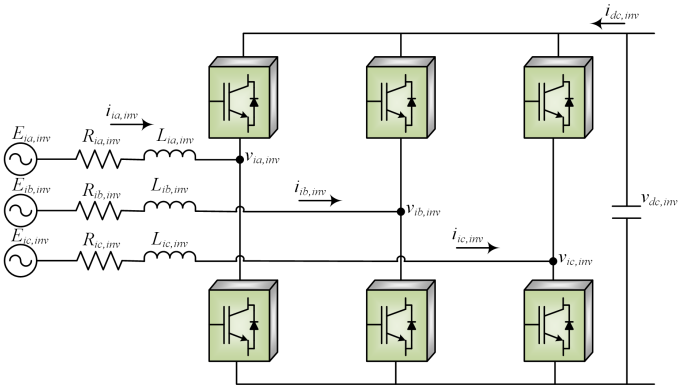

Fig. 4: Interlinking Voltage source converter design

in this work. In the review, key insights are provided about numerous characteristics. Safety, efficiency, steadfastness, and reliability, as well as the associated tradeoffs. Furthermore, this study presented how the interaction between availability and reliability, based on optimizing computational rate and restoring, drives reconfigurability.

On the DC source side, KVL may be applied to the microgrid system equation. One example of a DC source is attached to a battery that can provide a continuous voltage. In addition, [35] states that a constant power load is a DC load. The DC source voltage is equal to the total of the load voltage and the potential difference across the line loss, as stated by KVL at the DC MG.

$$V_{i,dc} = i_{i,dc} R_{i,dc} + V_{i,dc,load} \tag{18}$$

For constant power load, $P_{i,dc,load}$ will remain unchanged which can be expressed as.

$$V_{i,dc} = i_{i,dc} R_{i,dc} + \frac{P_{i,dc,load}}{i_{i,dc,load}} \tag{19}$$

III. Proposed Adaptive NN Control for SMG

Figure 4 presents on board hybrid MG's two-level voltage source converter (VSC) model. For the hierarchical control application, a two-level VSC system is used. There are two loops in the control system, one for the current and one for the voltage. Regulation of voltage is accomplished by the use of a PI controller in the secondary controller. It is also possible to regulate the main layer using a loop that depends on the current flow ($V-Q$). The expression for the inverter terminal voltage v_{inv} is as follows.

$$v_{i,inv} = E_{i,inv} + R i_{i,inv} + L_{i,inv} \frac{\mathrm{d}}{\mathrm{d}t} i_{i,inv} \tag{20}$$

Here, the inverter line impedance rate of change and the inverter transient voltage $E_{i,inv}$ are the two variables that combine to produce the inverter terminal voltage $v_{i,inv}$. The three-phase voltages on the VSC are $E_{a,inv}$, $E_{b,inv}$, and $E_{c,inv}$. The three-phase root mean square (RMS) voltage $E_{i,inv}$ may be drawn from the AC bus or a three-phase transformer, eliminating the need for a double voltage capacitor. After

the transits, the root-mean-square voltage at $E_{i,inv}$ will be steady and consistent regardless of the conditions. Prior to the load being connected to the AC bus, an LC filter network is established [36]. This project does not include filter design. For this reason, we refer to them in our formulations as constants.

$$\frac{\mathrm{d}}{\mathrm{d}t}i_{i,inv} = \frac{v_{i,inv}}{L_{i,inv}} - \frac{R_{i,inv}}{L_{i,inv}}i_{i,inv} - \frac{E_{i,inv}}{L_{i,inv}} \tag{21}$$

Applying dq-transformation of three phase currents.

$$\frac{\mathrm{d}}{\mathrm{d}t}i^d_{i,inv} = \frac{v^d_{i,inv}}{L_{i,inv}} - \frac{E^d_{i,inv}}{L_{i,inv}} + \omega_i i^q_{i,inv} - \frac{R_{i,inv}}{L_{i,inv}}i^d_{i,inv} \tag{22}$$

and

$$\frac{\mathrm{d}}{\mathrm{d}t}i^q_{i,inv} = \frac{v^q_{i,inv}}{L_{i,inv}} - \frac{E^q_{i,inv}}{i,L_{inv}} - \omega_i i^d_{i,inv} - \frac{R_{i,inv}}{L_{i,inv}}i^q_{i,inv} \tag{23}$$

The state space model of (22) and (23) can be represent as

$$\dot{x}_{i,inv} = A_{inv}x_{i,inv} + B_{inv}x_{i,inv} + D_{inv}E_{i.inv} \tag{24}$$

$$\begin{bmatrix}\dot{x}_1\\ \dot{x}_2\end{bmatrix} = \begin{bmatrix}-\frac{R_{i,inv}}{L_{i,inv}} & \omega_i\\ -\omega_i & -\frac{R_{i,inv}}{L_{i,inv}}\end{bmatrix}\cdot\begin{bmatrix}x_1\\ x_2\end{bmatrix} + \frac{1}{L_{inv}}\begin{bmatrix}u_1\\ u_2\end{bmatrix} - \frac{1}{L_{inv}}\begin{bmatrix}E^d_{i,inv}\\ E^q_{i,inv}\end{bmatrix} \tag{25}$$

Based on the characteristics of the coefficient matrix A, it can be concluded that the system will be stable for all time. Assuming all initial values and inputs are set to zero, we obtain.

$$\dot{x}_1 = -\frac{R_{i,inv}}{L_{i,inv}}x_1 + \omega_i x_2 \tag{26}$$

$$\dot{x}_2 = -\omega_i x_1 - \frac{R_{i,inv}}{L_{i,inv}}x_2 \tag{27}$$

The proposed control and power sharing strategy is given as

$$DG_i = \begin{cases} v^*_{i,d} = & v_{ref} - u_{i,q}\\ v^*_{i,q} = & 0\\ f_i = & f_{i,freq} - u_{i,p}\end{cases} \tag{28}$$

The dq transformed output error equations can be given as

$$e^d_{inv} = i^*_{i,ac,load} - i^d_{i,d,ac,load} = x^*_{i,1} - x_{i,1} \tag{29}$$

$$e^q_{inv} = i^*_{i,ac,load} - i^q_{i,ac,load} = x^*_{i,2} - x_{i,2} \tag{30}$$

and

$$\dot{e}^d_{inv} = -\dot{i}^d_{i,ac,load} = -\dot{x}_{i,1} \tag{31}$$

$$\dot{e}^q_{inv} = -\dot{i}^q_{i,ac,load} = -\dot{x}_{i,2} \tag{32}$$

A. Adaptive tracking

Choosing a quadratic lyapunov function candidate as

$$V = \frac{1}{2}\sum_{i=1}^{N} V_i^2 \tag{33}$$

we get

$$V = \frac{1}{2}\sum_{i=1}^{N}(x^2_{i,1} + x^2_{i,2}) \tag{34}$$

By taking derivatives

$$\dot{V} = \frac{1}{2}\sum_{i=1}^{N}(2x_{i,1}\dot{x}_{i,1} + 2x_{i,2}\dot{x}_{i,2}) \tag{35}$$

or

$$\dot{V} = \sum_{i=1}^{N}(x_{i,1}\dot{x}_{i,1} + x_{i,2}\dot{x}_{i,2}) \tag{36}$$

Now applying the adaptive state feedback control

$$u = -Kx_i \tag{37}$$

Condition need to satisfy

$$x_1 g_1(x) - x_2 g_2(x) < \sum_{i=1}^{2} x_i g_i(x) \tag{38}$$

For adaptive tracking error will become

$$e^d_{inv} = i^*_{i,ac,load} - Ki^d_{i,d,ac,load} = x^*_{i,1} - Kx_{i,1} \tag{39}$$

$$e^q_{inv} = i^*_{i,ac,load} - Ki^q_{i,ac,load} = x^*_{i,2} - Kx_{i,2} \tag{40}$$

The derivative terms of e^d_{inv} and e^q_{inv} can be given as

$$\dot{e}^d_{inv} = -K\dot{i}^d_{i,ac,load} = -K\dot{x}_{i,1} \tag{41}$$

$$\dot{e}^q_{inv} = -K\dot{i}^q_{i,ac,load} = -K\dot{x}_{i,2} \tag{42}$$

Solving the lyapunov function as

$$V = \frac{1}{2}\sum_{i=1}^{N}(e^2_{i,1} + e^2_{i,2}) \qquad \because N = 2 \tag{43}$$

Taking derivative

$$\dot{V} = \frac{1}{2}\sum_{i=1}^{N}(2e_{i,1}\dot{e}_{i,1} + 2e_{i,2}\dot{e}_{i,2}) \tag{44}$$

Simplifying

$$\dot{V} = \sum_{i=1}^{N}(e_1\dot{e}_1 + e_{i,2}\dot{e}_{i,2}) \tag{45}$$

Generalized form can be represented as

$$\dot{V} = \sum_{i=1}^{N}(e_i\dot{e}_i) \tag{46}$$

By putting values from (39), (40), (41) and (42) in (45), we get

$$\dot{V} = \sum_{i=1}^{N}(x_{i,1}^{*} - Kx_{i,1})(-K\dot{x}_{i,1}) + (x_{i,2}^{*} - Kx_{i,2})(-K\dot{x}_{i,2}) \tag{47}$$

Rearranging the equation

$$\dot{V} = \sum_{i=1}^{N}(-x_{i,1}^{*}\dot{x}_{i,1} - x_{i,2}^{*}\dot{x}_{i,2}) + K\sum_{i=1}^{N}\{(x_{i,1}\dot{x}_{i,1}) + (x_{i,2}\dot{x}_{i,2})\} < 0 \tag{48}$$

Here,

$$K\sum_{i=1}^{N}\{(x_{i,1}\dot{x}_{i,1}) + (x_{i,2}\dot{x}_{i,2})\} < 0 \quad \forall |x_i| \tag{49}$$

Hence, the proposed controller will guarantee an adaptive and stabilizing controller for the shipboard microgrid.

IV. Simulation Results

Simulation tests were conducted to evaluate the performance of the proposed controller for a hybrid microgrid. In this simulation, we employed two identical models of the hybrid MG1 and MG2. Considering 2 kW active loads having 1 $kVar$, inductive load is linked in parallel with circuit breakers and lumped impedances in the transmission line. The AC side microgrid operated at a frequency of 50 Hz and was connected to a distribution transformer and LCL filter units, enabling it to share power with the DC side microgrid through an IC. The IC between AC/DC microgrid is operating as a 2-level VSC, allowing bidirectional power flow based on load requirements.

Conversely, the DC microgrid includes DC sources such as BESS and PV solar panels, alongside DC resistive loads and transmission line resistance. The nominal voltage for the DC microgrid was set at 550 volts, with 6 kW resistive loads connected with circuit breakers.

The core objective of the adaptive hierarchical secondary controller is to monitor the line current information for both MG1 and MG2 to generate reference signals for their local primary droop controllers. The implementation and testing of this proposed controller were carried out using MATLAB/Simulink. The simulation parametric values are given in Table I.

The simulation aimed to compare the performance of conventional proportional integral (PI) and adaptive control based secondary controller with the proposed NN based secondary control strategies for the hybrid SMGs. Specifically, we focused on the transition from MG1 to MG2, which occurred at simulation time $t = 0.5$ sec. Prior to this transition $0 < t < 0.5$ sec, both the MG1 and MG2 were powered by the DC source, supplying power to both MG1 and MG2 loads. After $t = 0.5$ sec, the DC source of MG2 took over, providing power to both MG1 and MG2 loads from $t = 0.5$ sec to $t = 1.0$ sec.

TABLE I: Hybrid microgrid system parameters

Parameters	Description	Values
P_{load}	Active power	2 kW each
Q_{load}	Reactive power	1 kVar each
$v_{ac,s}$	Voltage	400 volts
$P_{ac,s}$	Rated power of DG	16 kVA
f_{load}	Frequency	50 Hz
$P_{dc,load}$	DC Load power	6 kW
$v_{dc,bus}$	DC bus Voltage	550 volts

A. Case 1 : Power flow from AC to DC side with load increments

Figure 5 (a) illustrates the power variation of AC loads within the hybrid microgrid. Initially, a main grid is providing power to both the MG1 and MG2. Here, we can see smooth power flow during $0.5 < t < 1.0$ sec. Subsequently, the main grid is disconnected at $t = 0.5$ sec. Now, the power demand needs to be fulfilled within the microgrids. Therefore, MG1 starts providing the power to both the MG1 and MG2 without the interception. In this case, we determined that the suggested secondary control, which is based on adaptive control, performed better than the traditional controllers by a considerable margin. The load power is accurately controlled and tracked when the adaptive controller is used at t>0.5 sec.

Figure 5 (b) shows the reactive power variations during the microgrid transitions. Here, we can observe that the performance of reactive power by applying an adaptive secondary controller is smart as compared to the other controllers.

Figure 5 (c) depicts the frequency variations on the AC grid. In this context, the frequency control achieved by the adaptive controller results in better frequency regulation and a stable response compared to conventional control methods. While both the PI and adaptive controllers exhibit frequency variations, the adaptive controller effectively maintains a smooth regulation at 50 Hz. The frequency droop due to change over is observed $\Delta\ f^{1}_{droop} = 0.05\ Hz$, $\Delta f^{2}_{droop} = 0.085\ Hz$ and $\Delta f^{3}_{droop} = 0.1\ Hz$.

Figure 7 (d) shows the DC load power of both MG1 and MG2. We can see that both DC load of MG1 and MG2 are stable and regulated to 6 kW. Furthermore, the DC load power is not much influenced by grid transitions.

B. Case 2 : Power flow from AC to DC side then DC to AC side with load variations

Figure 6 (a) illustrates a comparison between the traditional approach and the proposed adaptive secondary controller in terms of AC load power fluctuations resulting from microgrid transition and load changes. Initially, a main grid is providing power to both the MG1 and MG2. Here, we can see smooth power flow during $0.5 < t < 1.0$ sec. Moreover, a 2 kW load increased at $t = 0.25$ sec, which can be seen in the plot. Subsequently, the main grid is disconnected at $t = 0.5$ sec. Now, the power demand needs to be fulfilled within the microgrids. Therefore, MG1 starts providing the power to both the MG1 and MG2 without the interception.

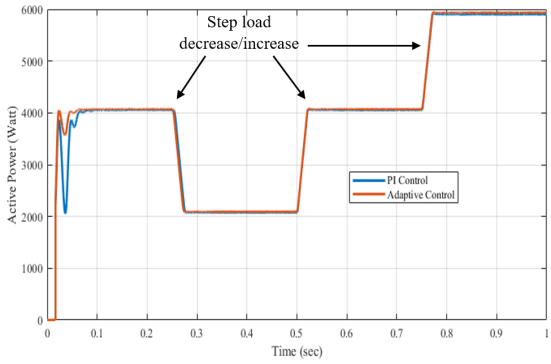

(a) Active power variations (P_{load})

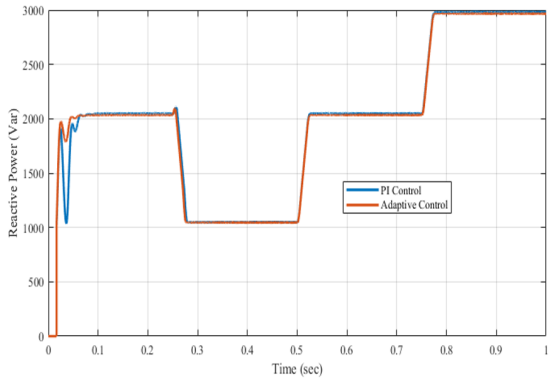

(b) Reactive power (Q_{load})

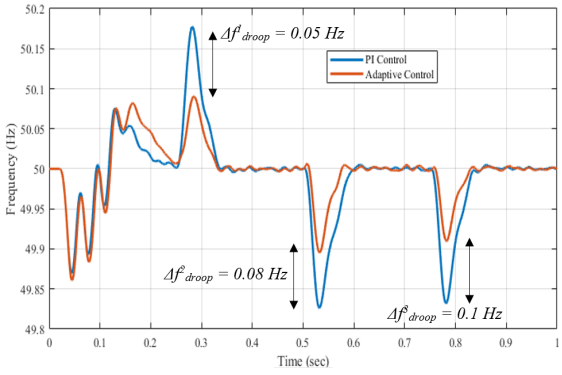

(c) Frequency variations (f_{load})

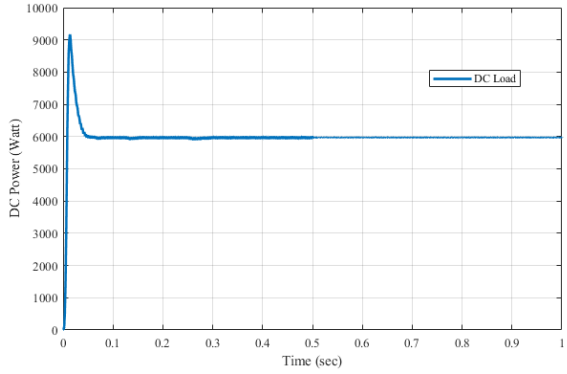

(d) DC Load Power(P_{DC})

Fig. 5: Case 1 : Power flow from MG1 to MG2 side with load increments

In this case, we observed the performance of the proposed adaptive secondary control is significantly better than of the conventional controllers. At t>0.5 sec, the load power is precisely regulated at 6 kW load demand when using the adaptive controller then reduces to 4 kW at $t = 0.75$ sec. Consequently, the dip in load power amounts to $\Delta P_{load}^{adaptive} = 150$ W and $\Delta P_{load}^{PI} = 1520$ W. lastly, the 2 kW load removed at $t = 0.75$ sec which can be seen in plot.

Figure 6 (b) shows the reactive power variations during the microgrid transitions. Here, we can observe that the performance of reactive power by applying an adaptive secondary controller is optimal as compared to the other controllers. The reactive power variation can be measured for proposed and conventional controllers are $\Delta P_{load}^{adaptive} = 470$ Var and $\Delta P_{load}^{PI} \approx 1150$ Var.

In Figure 6 (c), a comparison is made between conventional and proposed secondary controllers, focusing on frequency variations resulting from microgrid transition as well as load power increments. The 2 kW step load increases at $t = 0.25$ sec and decreases at $t = 0.75$ sec. Here, it is evident that the utilization of a secondary controller strategy leads to an enhancement in the frequency droop response, which is $\Delta f_{load}^{adaptive} = 0.18$ Hz compared to $\Delta f_{load}^{PI} \approx 0.23$ Hz.

Figure 6 (d) shows the DC load power of both MG1 and MG2. We can see that both DC load of MG1 and MG2 are stable and regulated to 6 kW.

V. Hardware Implementations

A computer may be taught to do a certain task by providing it with a small set of examples. The Turing test is one of several methods for determining if a computer system has intelligence. In electronic communication, two identities, a person and a computer, are involved. Decisions are often made by a permanently installed traditional algorithm that takes sensor data, human inputs, and trigger events into account. A human being is required to code any computer software. The problem is that this approach becomes obsolete very fast due to the more complicated computing needs of today. Computer experts were the first to notice this issue. Figure 7 (a) shows the block diagram of the hardware and Figure 7 (b) shows the hardware setup of our proposed design.

1) Supervised learning: Supervised learning involves explicitly telling the machine what to learn. Following the analysis of a large-scale training dataset, the system seeks structures that may be used for object distinction. By observing these structures, the system may train itself to differentiate between different sets of data.

2) Unsupervised learning: For a system to learn unsupervised, it must be able to function without explicit human instructions. It analyses the given data on its own and looks for trends and regularities. If the data is comparable, it might provide equal results. This method shows much promise when dealing with data that has several components, such as the words in a phrase. Assuming everything goes well, the values of individual words may be utilized to forecast the subsequent component.

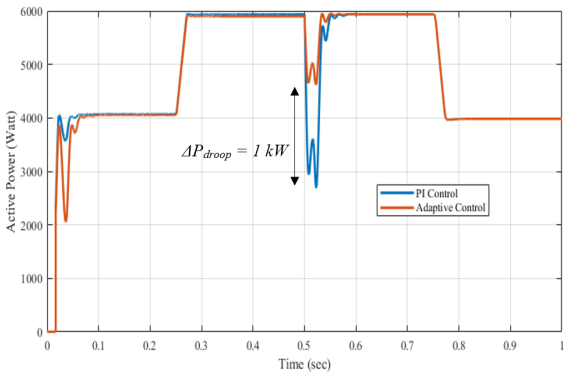

(a) Active power variations (P_{load})

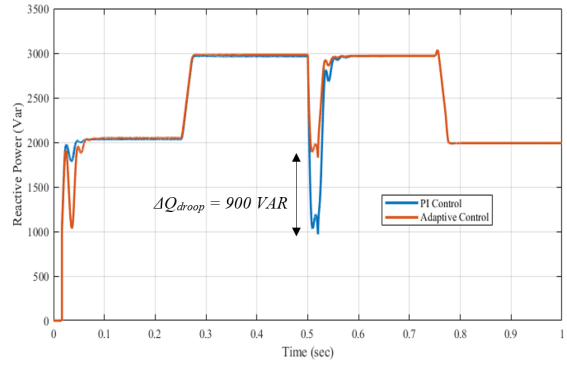

(b) Reactive power (Q_{load})

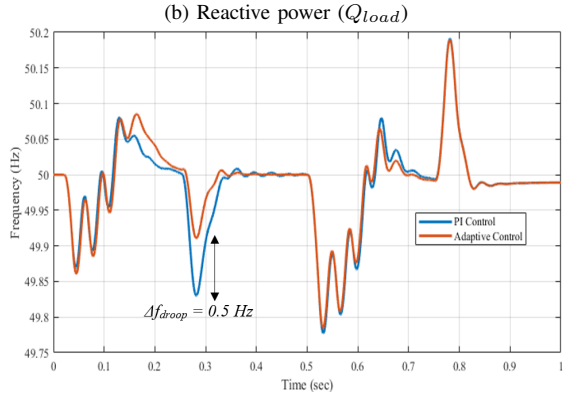

(c) Frequency variations (f_{load})

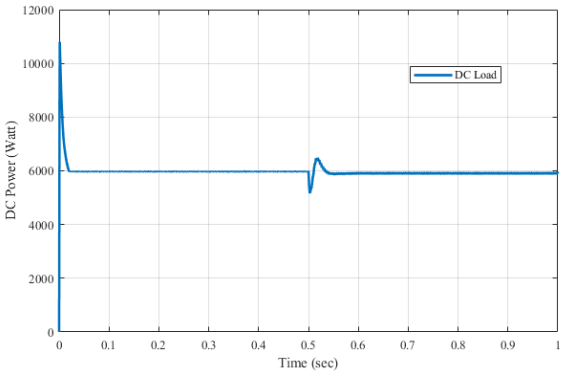

(d) DC Load Power(P_{DC})

Fig. 6: Case 2 : Power flow from MG1 to MG2 side then MG2 to MG1 side with load variations

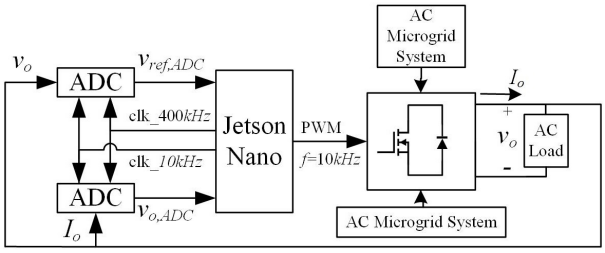

(a) Hardware block diagram

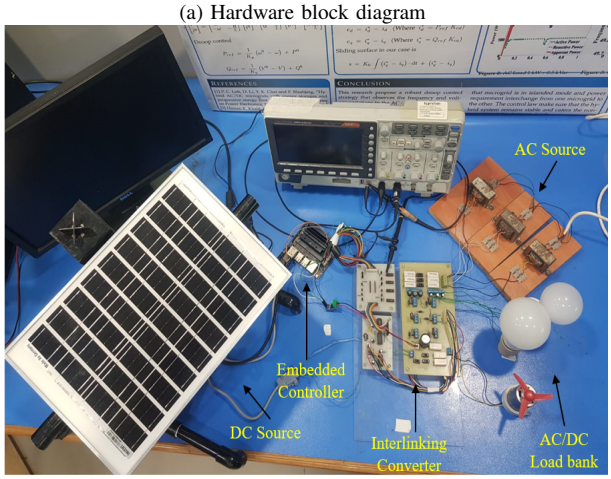

(b) Hardware setup

Fig. 7: Hardware Design

3) Reinforcement learning: The algorithm used in reinforcement learning has to carry out a sequence of operations before it can determine the outcome.

4) Deep learning: Deep learning is a specific kind of machine learning, according to the technical definition, which is modeled after the way the human brain functions biologically, artificial neural network (ANN). The three main components of an ANN architecture are the input, obscured, and output layers. Their structures are typically directed graphs, regardless of how complicated. A deep learning ANN is one that contains many concealed layers and a very deep structure.

Data records organized in a structured format may be retrieved from a database. The data is automatically recognized by machine learning, which then creates its own algorithms to categorize the items. In order to classify things in photos, the deep learning algorithm must first identify unknown structures in the input data. From there, it builds a complicated model for the purpose of attaining a high standard of model quality. Having said that, massive volumes of data are needed for this approach.

A. NVIDIA Jetson Nano System

An introduction to the idea of AI is provided via the Jetson Nano programming board from NVIDIA. As a result, AI systems that are both economical and environmentally friendly may be created. A new world of opportunities has opened up with the single-board computer that has four ARM cores and the Maxwell graphics processing unit (GPU), which acts as

a CUDA computing accelerator and video engine. There are two Jetson Nano models available from NVIDIA. The main distinctions between them are the amount of RAM (4 GB), the display connector, and the power interface. The Jetson gadget is called Jetson Nano-Module, which measures around 70 x 45 mm. When it comes to AI, this production-ready System-on-Module (SOM) has several benefits for many industries: Its 472 GFLOPs make it ideal for running state-of-the-art AI algorithms rapidly. It is possible to analyze data from many high-resolution sensors simultaneously and run multiple neural networks in parallel. These features make it a great choice for intelligent gateways that can do comprehensive analytics, entry-level network video recorders, and homemade robotics.

B. Hardware Results

Figure 8 shows the hardware results waveform achieved during the experimenting of the proposed adaptive NN and conventional PI based control schemes. Figure 8 (a) shows the load active power variation due to the gird transition from AC side to DC side of the microgrid. We can see that at time $t = 0.25\ sec$, there is a step load increment from $4\ kW$ to $6kW$. Afterward, a voltage droop occurs at $t = 0.5\ sec$, where we can see that the performance of the adaptive controller is better than the conventional control scheme. The ΔP_{droop} observed is $1.4\ kW$. The frequency variations are shown in Figure 8 (b). Here, frequency droops were observed due to load variation and grid transitions. Figure 8 (c) shows DC load power which is regulated at $950\ W$. We observed $P_{dc,droop} = 120\ W$ at $t = 0.5\ sec$ due to grid transition.

VI. Conclusions

The hybrid AC/DC microgrid system is a possible solution for the increasing demand for power with distributed generators, storage systems, and loads. This paper is focused on the growing trend of adaptive NN-based control design for the hybrid microgrid system due to the utilization of both AC and DC sources and loads. It aims at developing a SMG system combining both in a layout structure to improve the system flexibility/efficiency. This research demonstrated the necessary role of Adaptive NN in addressing complex control problems associated with SMGs. The results validate that adaptive NN-based control strategies will play a vital role in the next phase of hybrid microgrids. The novelty of this work lies in its unique approach to combining AC and DC elements within a microgrid, enhancing system flexibility and efficiency.

The AI-based control scheme leverages advanced functionalities such as decision-making, machine learning, and inference to address the complex control problems inherent in hybrid microgrids. The practical validation through simulations further underscores the effectiveness of the proposed intelligent control scheme, highlighting its potential to revolutionize the operation and management of modern power systems. The platform of the proposed AI-based controller not only improves the microgrid's operational reliability but also ensures that it is a better, more robust, and flexible power system application.

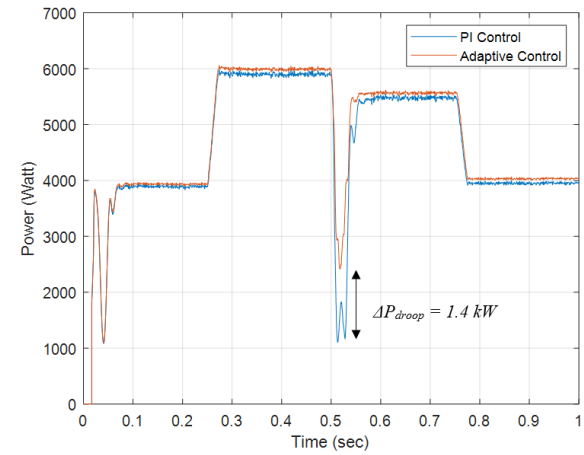

(a) Active power variations at AC load

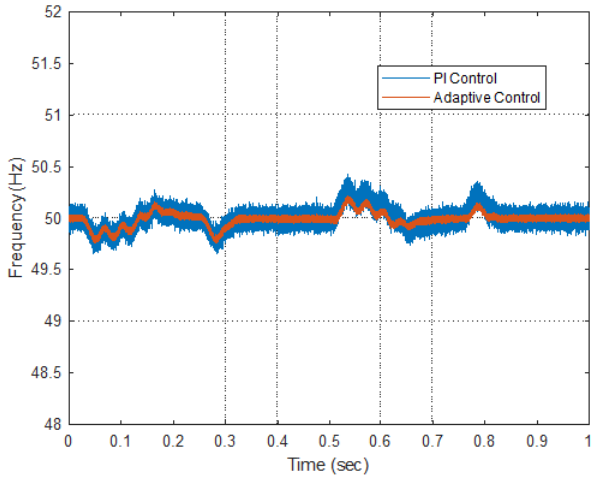

(b) Frequency variations at AC load

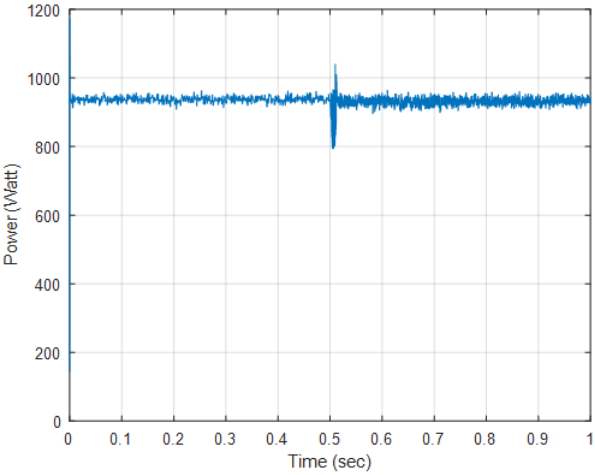

(c) DC load voltage variations

Fig. 8: Practical results of power flow from AC to DC side then DC to AC side comparisons

REFERENCES

[1] Kiran, N. (2014). Sliding Mode Control of Buck Converter. Buletin Teknik Elektro dan Informatika(Bulletin of Electrical Engineering and Informatics), 37-44..

[2] Saoudi, M., El-Sayed, A., Metwally, H. (2017). Design and Implementation of Closed-Loop Control System for Buck converter Using different techniques. IEEE A and E SYSTEMS MAGAZINE, 30-39.

[3] Das, A.,Namboothiripad, M. K. (2014). Voltage Control of Buck Converter using Sliding Mode Controller. International Journal of Engineering Research Technology (IJERT), 1619-1623.

[4] Hashmi, S. M., Memon, A. Y. (2020). Simulation of PWM based Sliding Mode Controller for a DC-DC Buck Converter on FIL. IEEE Xplore, 344-349.

[5] A. Rehmat, F. Alam, M. Nasir and S. S. Zaidi, "Robust Hierarchical Non-linear Droop Control Design for the PV based Islanded Microgrid," 2022 19th International Bhurban Conference on Applied Sciences and Technology (IBCAST), Islamabad, Pakistan, 2022, pp. 620-628, doi: 10.1109/IBCAST54850.2022.9990397.

[6] Yamashita, Daniela Yassuda, Ionel Vechiu, and Jean-Paul Gaubert. "A review of hierarchical control for building microgrids." Renewable and Sustainable Energy Reviews 118 (2020): 109523.

[7] Ali, Waleed, et al. "Hierarchical control of microgrid using IoT and machine learning based islanding detection." IEEE Access 9 (2021): 103019-103031.

[8] Khan, Shahzad, et al. "Artificial intelligence framework for smart city microgrids: State of the art, challenges, and opportunities." 2018 third international conference on Fog and Mobile Edge Computing (FMEC). IEEE, 2018.

[9] Chui, Kwok Tai, Miltiadis D. Lytras, and Anna Visvizi. "Energy sustainability in smart cities: Artificial intelligence, smart monitoring, and optimization of energy consumption." Energies 11.11 (2018): 2869.

[10] Nair, Divya R., Manjula G. Nair, and Tripta Thakur. "A smart microgrid system with artificial intelligence for power-sharing and power quality improvement." Energies 15.15 (2022): 5409.

[11] Sabzehgar, Reza, Diba Zia Amirhosseini, and Mohammad Rasouli. "Solar power forecast for a residential smart microgrid based on numerical weather predictions using artificial intelligence methods." Journal of Building Engineering 32 (2020): 101629.

[12] Hasija, Sameer, and Chung Piaw Teo. "Introduction to the Special Section on Smart City Operations." Manufacturing & Service Operations Management 24.5 (2022): 2387-2388.

[13] Mohammadi, Ebrahim, et al. "A review on application of artificial intelligence techniques in microgrids." IEEE Journal of Emerging and Selected Topics in Industrial Electronics (2022).

[14] Jayashree, S., and K. Malarvizhi. "AI-Based Smart Micro Grids." Advanced Controllers for Smart Cities. Springer, Cham, 2021. 1-14.

[15] Kundu, Debasish. "Blockchain and trust in a smart city." Environment and Urbanization ASIA 10.1 (2019): 31-43.

[16] Albarakati, Aiman J., et al. "Real-time energy management for DC microgrids using artificial intelligence." Energies 14.17 (2021): 5307.

[17] Omitaomu, Olufemi A., and Haoran Niu. "Artificial intelligence techniques in smart grid: A survey." Smart Cities 4.2 (2021): 548-568.

[18] Omitaomu, Olufemi A., and Haoran Niu. "Artificial intelligence techniques in smart grid: A survey." Smart Cities 4.2 (2021): 548-568.

[19] Kanase-Patil, Amarsingh B., et al. "A review of artificial intelligence-based optimization techniques for the sizing of integrated renewable energy systems in smart cities." Environmental technology reviews 9.1 (2020): 111-136.

[20] Herath, Pramod Uthpala, et al. "Computational intelligence-based demand response management in a microgrid." IEEE Transactions on Industry Applications 55.1 (2018): 732-740.

[21] Song, Yonghua, et al. "Resilient power grid for smart city." iEnergy 1.3 (2022): 325-340.

[22] Nammouchi, A., Aupke, P., Kassler, A., Theocharis, A., Raffa, V., & Di Felice, M. (2021, September). Integration of AI, IoT and edge-computing for smart microgrid energy management. In 2021 IEEE International Conference on Environment and Electrical Engineering and 2021 IEEE Industrial and Commercial Power Systems Europe (EEEIC/I&CPS Europe) (pp. 1-6). IEEE.

[23] Mar´ın Quintero, J. G. (2022). Adaptive protection in active distribution networks using local information.

[24] Sarangi, R. R., Pradhan, A., Moharana, J., Ray, P. K., & Mohanty, A. (2023, December). Rate of Change of Frequency Detection in Microgrid under Stochastic Supply and Load. In 2023 IEEE 3rd International Conference on Smart Technologies for Power, Energy and Control (STPEC) (pp. 1-5). IEEE

[25] Marin-Quintero, J., Orozco-Henao, C., Bretas, A. S., Velez, J. C., Herrada, A., Barranco-Carlos, A., & Percybrooks, W. S. (2022). Adaptive fault detection based on neural networks and multiple sampling points for distribution networks and microgrids. Journal of Modern Power Systems and Clean Energy, 10(6), 1648-1657.

[26] Rodriguez, D. F., Alvarez, D. L., Gomez, D., Gers, J. M., & Rivera, S. (2021, February). Low-cost analysis of load flow computing using embedded computer empowered by gpu. In 2021 IEEE Power & Energy Society Innovative Smart Grid Technologies Conference (ISGT) (pp. 1-5). IEEE

[27] Gozuoglu, A., Ozgonenel, O., & Gezegin, C. (2024). CNN-LSTM Based Deep Learning Application on Jetson Nano: Estimating Electrical Energy Consumption for Future Smart Homes. Internet of Things, 101148.

[28] Trivedi, R., & Khadem, S. (2022). Implementation of artificial intelligence techniques in microgrid control environment: Current progress and future scopes. Energy and AI, 8, 100147.

[29] Wu, T., & Wang, J. (2021). Artificial intelligence for operation and control: The case of microgrids. The Electricity Journal, 34(1), 106890

[30] Wu, T., & Wang, J. (2021). Artificial intelligence for operation and control: The case of microgrids. The Electricity Journal, 34(1), 106890.

[31] Akpolat, A. N., Habibi, M. R., Dursun, E., Kuzucuoglu, A. E., Yang, Y., ˘ Dragicevi ˘ c, T.,& Blaabjerg, F. (2020). Sensorless control of DC microgrid ´based on artificial intelligence. IEEE Transactions on Energy Conversion, 36(3), 2319-2329

[32] Nair, D. R., Nair, M. G., & Thakur, T. (2022). A smart microgrid system with artificial intelligence for power-sharing and power quality improvement. Energies, 15(15), 5409.

[33] Chaurasia, K., & Kamath, H. R. (2021, April). New Approach using Artificial Intelligence-Machine Learning in Demand Side Management of Renewable Energy integrated Smart Grid for Smart City. In Proceedings of the International Conference on Innovative Computing & Communication (ICICC).

[34] Cabrera, W., Benhaddou, D., & Ordonez, C. (2016, May). Solar power prediction for smart community microgrid. In 2016 IEEE international conference on smart computing (SMARTCOMP) (pp. 1-6). IEEE.

[35] Altin, N., & Eyimaya, S. E. (2023, June). Artificial intelligence applications for energy management in microgrid. In 2023 11th International Conference on Smart Grid (SmartGrid) (pp. 1-6). IEEE.

[36] Manolescu, D., Reid, D., & Secco, E. L. (2024, March). Hardware and Software Integration of Machine Learning Vision System Based on NVIDIA Jetson Nano. In Future of Information and Communication Conference (pp. 129-137). Cham: Springer Nature Switzerland.